

## High spatial resolution subsurface thermal emission microscopy

S. B. Ippolito,<sup>a)</sup> S. A. Thorne, M. G. Eraslan, B. B. Goldberg, and M. S. Ünlü

*Department of Physics and Electrical and Computer Engineering and the Photonics Center, Boston University, 8 Saint Mary's Street, Boston, Massachusetts 02215*

Y. Leblebici

*Microelectronic Systems Laboratory, Swiss Federal Institute of Technology, CH-1015 Lausanne, Switzerland*

(Received 23 January 2004; accepted 4 April 2004; published online 14 May 2004)

We apply the numerical aperture increasing lens technique to subsurface thermal emission microscopy of Si integrated circuits. We achieve improvements in the amount of light collected and the spatial resolution, well beyond the limits of conventional thermal emission microscopy. We experimentally demonstrate a lateral spatial resolution of  $1.4\ \mu\text{m}$  and a longitudinal spatial resolution of  $7.4\ \mu\text{m}$ , for thermal imaging at free space wavelengths up to  $5\ \mu\text{m}$ . © 2004 American Institute of Physics. [DOI: 10.1063/1.1758308]

A thermal emission microscope measures the temperature of an object by collecting mid-infrared photons incoherently radiated from that object. The Stefan–Boltzmann Law states that an object in thermal equilibrium, with constant emissivity, radiates a total optical power proportional to its absolute temperature to the fourth power. An object that has a spatial distribution of temperature is, by definition, not in thermal equilibrium. Such an object may, however, be divided into microscopic volumes that have the same temperature and are each in thermal equilibrium. A thermal emission microscope measures the local temperature of each microscopic volume by independently collecting the light radiated by that volume. Unlike scanning thermal microscopy,<sup>1</sup> micro-Raman spectroscopy,<sup>2</sup> thermoreflectance,<sup>3</sup> and other thermal microscopy techniques,<sup>4,5</sup> thermal emission microscopy is the only passive technique that can directly measure the temperatures of subsurface volumes.

In semiconductor failure analysis, a thermal emission microscope is an invaluable tool for mapping the temperatures of Si integrated circuits (Si ICs). Thermal radiation from a Si IC with constant emissivity is primarily at mid-infrared wavelengths, with a peak at a wavelength between  $6\ \mu\text{m}$  and  $10\ \mu\text{m}$ , at typical temperatures in failure analysis, between  $200\ ^\circ\text{C}$  and  $20\ ^\circ\text{C}$ , respectively. Most thermal emission microscopes employ an InSb detector or a PtSi charge coupled device camera, detecting light at free space wavelengths up to  $5\ \mu\text{m}$ . Thus, most of the signal results from light at free space wavelengths between  $4\ \mu\text{m}$  and  $5\ \mu\text{m}$ . Current Si IC technology includes many opaque metal layers and structures above semiconductor devices, thereby hindering topside thermal emission microscopy of these buried devices in their final state. Thus, backside thermal emission microscopy through the Si substrate is used almost exclusively in failure analysis. Additionally, most thermal radiation propagates into the Si substrate, because of the Si substrate's high refractive index at mid-infrared wavelengths. At a free space wavelength ( $\lambda_0$ ) of  $5\ \mu\text{m}$ , the refractive index ( $n$ ) of Si is 3.43. The Si substrate is both transparent and homogeneous at mid-infrared wavelengths, allowing thermal

radiation to propagate through it. However, reflection and refraction of light at the planar surface of the Si substrate limits the amount of thermal radiation a thermal emission microscope can collect, as illustrated in Fig. 1(a). Reflection allows less than 3% of unpolarized light, uniformly emitted from a circuit, to escape the sample, according to the Fresnel formulae. Furthermore, much of the light that escapes the sample is refracted at high angles, which most thermal emission microscopes cannot collect because of their low numerical aperture. The absence of light from above the critical angle ( $\theta_c$ ), ultimately limits the lateral spatial resolution to  $2.5\ \mu\text{m}$  ( $\lambda_0/2n \sin \theta_c$ ) and the longitudinal spatial resolution to  $34\ \mu\text{m}$  ( $\lambda_0/n(1 - \cos \theta_c)$ ), for conventional thermal emission microscopes operating at free space wavelengths up to  $5\ \mu\text{m}$ .<sup>6</sup> Typical lateral spatial resolution values are about  $3\ \mu\text{m}$  for state-of-the-art commercial systems.<sup>7</sup> However, Si IC technology has reached submicron process size scales, well beyond the spatial resolution capability of conventional thermal emission microscopy. The large refractive index of Si at mid-infrared wavelengths offers the potential for significant improvement in the amount of light collected and the spatial resolution, if the planar barrier can be circumvented.

The addition of a numerical aperture increasing lens (NAIL),<sup>8,9</sup> a plano-convex optic, allows more light to escape, as illustrated in Fig. 1(b). The NAIL is made of Si, matching the refractive index of the Si substrate, so that light propagates from the Si substrate into the NAIL without refraction at the interface. After propagating through the NAIL, the light then refracts at the spherical surface into air, and is collected by a thermal emission microscope. For a substrate thickness ( $X$ ), the radius of curvature of the spherical surface

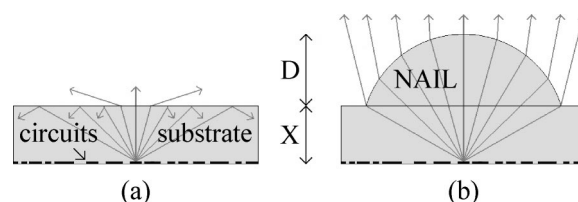


FIG. 1. Thermal emission from (a) a Si IC and (b) a Si IC with the addition of a NAIL.

<sup>a)</sup>Electronic mail: ippolito@bu.edu

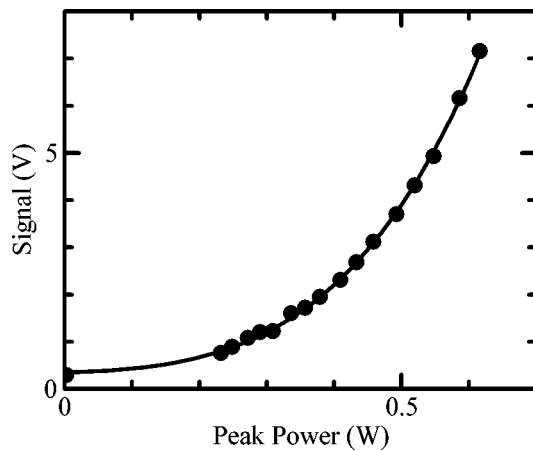


FIG. 2. The signal, as a function of the peak power applied to a  $2\ \mu\text{m}$  wide Al line, obeys the Stefan–Boltzmann law.

( $R$ ) and the center thickness ( $D$ ) of the NAIL are chosen by the relationship  $D + X = R(1 + 1/n)$ , so that the thermal image is spherical aberration free, or stigmatic.<sup>10</sup> A NAIL theoretically allows up to 63% of unpolarized light, uniformly emitted from a circuit, to reach a thermal emission microscope within a numerical aperture of 0.29. With a NAIL, our thermal emission microscope collected 8% of the light emitted from a circuit at best focus. This enhancement in the amount of light collected, compared to a theoretical maximum of 3% without a NAIL, greatly improves the thermal resolution of a thermal emission microscope. The diffraction of light theoretically limits the lateral spatial resolution to  $0.73\ \mu\text{m}$  and the longitudinal spatial resolution to  $1.5\ \mu\text{m}$ , for thermal emission microscopes with a NAIL, operating at free space wavelengths up to  $5\ \mu\text{m}$ . With a NAIL, we experimentally demonstrate a lateral spatial resolution of  $1.4\ \mu\text{m}$  and a longitudinal spatial resolution of  $7.4\ \mu\text{m}$ . Although we do not achieve the theoretical limits of NAIL microscopy, our experimental results represent a significant improvement over state-of-the-art conventional thermal emission microscopy.

Several issues caused our experimental results to fall short of the theoretical limits of NAIL microscopy. Conventional thermal emission microscopes are designed to minimize the effects of chromatic aberration over the range of mid-infrared wavelengths they collect. However, refraction at the spherical surface of a NAIL imparts a chromatic aberration proportional to  $R$ , which deteriorates the spatial resolution. Although the spacing between the substrate and the NAIL can be minimized by polishing both surfaces, a finite gap remains, since in practice the two surfaces are not perfectly planar. As the size of the gap increases monotonically with  $R$ , less light evanescently couples from the Si substrate across the gap into the NAIL. These two issues lead us to choose a smaller value of  $R$ , however, in doing so we reduce the numerical aperture of the NAIL. In our experiments, we attempted an optimization by choosing a value of  $R$  large enough to allow a numerical aperture of 2.7, but small enough to reduce the longitudinal chromatic aberration term to  $0.6\ \mu\text{m}$ . Also note that the gap, compared to previous experiments at near-infrared wavelengths,<sup>8</sup> has a smaller effect at mid-infrared wavelengths, because the evanescent decay length is proportional to the wavelength. A final issue,

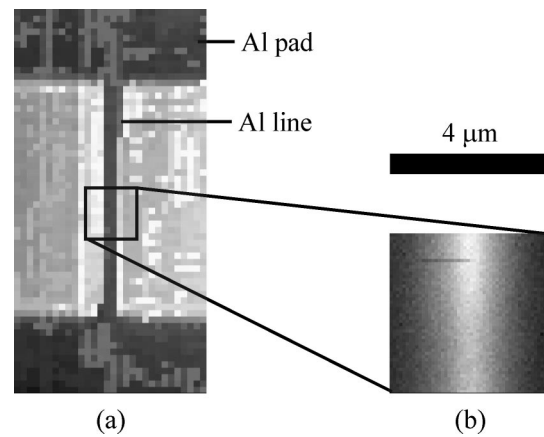


FIG. 3. (a) Inspection image of a  $0.8\ \mu\text{m}$  wide Al line, taken by an InGaAs camera and (b) thermal emission image of the Joule heating in the Al line, taken with an InSb detector at best focus.

common to all diffraction limited microscopes, is the tradeoff between the amount of light collected and the spatial resolution resulting from the size of the aperture or detector in the image space. We chose a detector size in our thermal emission microscope that demonstrates significant improvements in both quantities.

We built a thermal emission microscope, tailored for examination of a Si IC, using a NAIL. A computer controlled piezo stage is utilized to scan the Si IC and NAIL under the objective lens and the signal voltage is acquired using LABVIEW software. A lamp and a condenser lens below the stage provide illumination for visual inspection. Light from the Si IC and NAIL first encounters a mid-infrared, achromatic, objective lens with a numerical aperture of 0.25. A cold mirror then reflects near-infrared wavelengths to an InGaAs

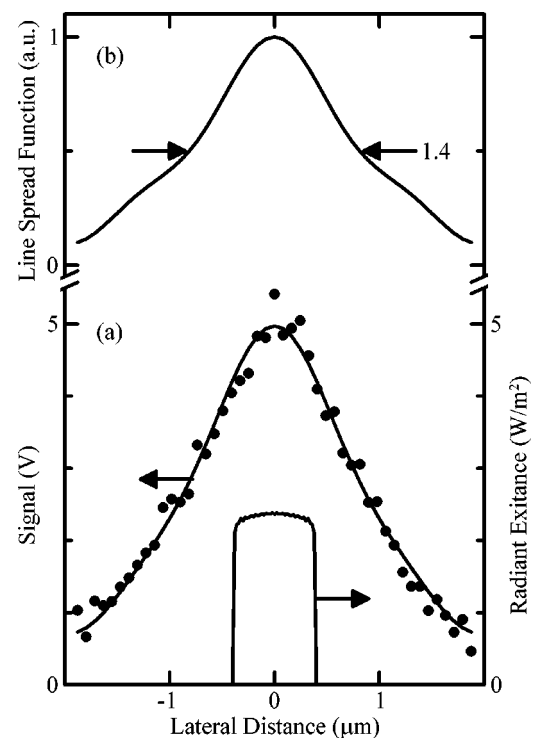


FIG. 4. (a) Signal and radiant exitance from a  $0.8\ \mu\text{m}$  wide Al line, as a function of lateral distance, and (b) resulting line spread function of the NAIL microscope with a FWHM of  $1.4\ \mu\text{m}$ .

camera for visual inspection, and transmits the mid-infrared wavelengths to a cooled,  $50\ \mu\text{m}$  diameter, InSb detector, which detects light at wavelengths from  $3\ \mu\text{m}$  to  $5\ \mu\text{m}$  for thermal emission microscopy. To test our thermal emission microscope, we fabricated a sample with passivated Al (1% Si) lines of varying widths and pads for electrical connection on a 1 mm thick Si wafer. We also had a matching Si NAIL manufactured with an  $R$  of 1.61 mm and a  $D$  of 1.07 mm. Joule heating an Al line generates a spatial distribution of temperature narrow enough to demonstrate a significant improvement in spatial resolution. We used a  $2\ \mu\text{m}$  wide Al line for most measurements, because it offers more thermal radiation and a better signal to noise ratio than a  $0.8\ \mu\text{m}$  wide Al line we used to test the lateral spatial resolution. The sample is flip chip bonded to a printed circuit board for connection and mounting to the piezo stage. The Al lines are driven by a sinusoidal voltage at a frequency of 900 Hz from a signal generator, while a lock-in amplifier measures the signal, which is the amplitude of the detector signal at the second harmonic of the drive voltage.

In our experiments, the signal levels are similar, with and without the NAIL, because the NAIL collects more light from the sample, but from a smaller volume. The signal, as a function of the peak power applied to the  $2\ \mu\text{m}$  wide Al line, obeys the Stefan–Boltzmann Law, as shown in Fig. 2. An inspection image of the  $0.8\ \mu\text{m}$  wide Al line, taken by the InGaAs camera, is shown in Fig. 3(a). A thermal emission image of the Joule heating in the Al line from a peak power of 0.058 W, taken with the InSb detector at best focus, is shown in Fig. 3(b). The signal, as a function of lateral distance, shown in Fig. 4(a), is a linecut from the thermal emission image in Fig. 3(b), and has a full width at half maximum (FWHM) of  $1.6\ \mu\text{m}$ . The simulated radiant exitance from the bottom surface of the Al line is also shown in Fig. 4(a). The line spread function shown in Fig. 4(b) is deconvolved from the signal and the simulated radiant exitance from the Al line. According to the Houston criterion, we demonstrate a lateral spatial resolution of  $1.4\ \mu\text{m}$ . In Fig. 5, the signal from the center of the  $2\ \mu\text{m}$  wide Al line, from a peak power of 0.36 W, as a function of longitudinal distance from best focus, has a FWHM of  $11.6\ \mu\text{m}$ . The collection focus is in the Si substrate for positive defocus values, and is below the Si/Al/air interface for negative defocus values, where the signal is the result of radiation from the sides of the Al line and reflection from the interface.<sup>11–13</sup> The FWHM of the signal, from the positive defocus values, indicates a longitudinal spatial resolution of  $7.4\ \mu\text{m}$ .

In summary, we have demonstrated the application of

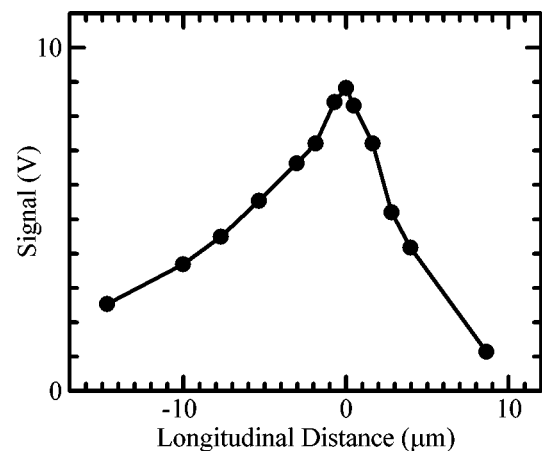


FIG. 5. Signal from the center of a  $2\ \mu\text{m}$  wide Al line, as a function of longitudinal distance from best focus.

NAIL technique to thermal emission microscopy, resulting in significant improvements. In subsurface thermal emission microscopy of Si ICs, we demonstrated improvements in both the lateral and longitudinal spatial resolutions, well beyond the limits of conventional thermal emission microscopy. Since the amount of light collected was not adversely affected by NAIL microscopy, while the resolution was improved, we believe that this technique will be widely used in thermal emission microscopy for semiconductor failure analysis.

This work was supported by Air Force Office of Scientific Research MURI F-49620-03-1-0379 and by NSF NIRT ECS-0210752.

- <sup>1</sup>A. Majumdar, *Annu. Rev. Mater. Sci.* **29**, 505 (1999).
- <sup>2</sup>S. Kouteva-Arguirova, T. Arguirov, D. Wolframm, and J. Reif, *J. Appl. Phys.* **94**, 4946 (2003).
- <sup>3</sup>G. Tessier, S. Holé, and D. Fournier, *Opt. Lett.* **28**, 875 (2003).
- <sup>4</sup>C. Pfügl, M. Litzberger, W. Schrenk, D. Pogany, E. Gornik, and G. Strasser, *Appl. Phys. Lett.* **82**, 1664 (2003).
- <sup>5</sup>J. Kölzer, E. Oesterschulze, and G. Deboy, *Microelectron. Eng.* **31**, 251 (1996).
- <sup>6</sup>C. J. R. Sheppard, *J. Microsc.* **149**, 73 (1988).
- <sup>7</sup>S. Kondo and K. Hinode, *Appl. Phys. Lett.* **67**, 1606 (1995).
- <sup>8</sup>S. B. Ippolito, B. B. Goldberg, and M. S. Ünlü, *Appl. Phys. Lett.* **78**, 4071 (2001).
- <sup>9</sup>B. B. Goldberg, S. B. Ippolito, L. Novotny, Z. Liu, and M. S. Ünlü, *IEEE J. Sel. Top. Quantum Electron.* **8**, 1051 (2002).
- <sup>10</sup>M. Born and E. Wolf, *Principles of Optics*, 7th ed. (Cambridge University Press, New York, 1999), pp. 465 and 159.
- <sup>11</sup>J.-J. Greffet, R. Carminati, K. Joulain, J.-P. Mulet, S. Mainguy, and Y. Chen, *Nature (London)* **416**, 61 (2002).
- <sup>12</sup>L. Novotny, R. D. Grober, and K. Karrai, *Opt. Lett.* **26**, 789 (2001).
- <sup>13</sup>L. Novotny, *J. Opt. Soc. Am. A* **14**, 91 (1997).